Research Square

Preprints are preliminary reports that have not undergone peer review.
They should not be considered conclusive, used to inform clinical practice,
or referenced by the media as validated information.

Integrated Remote Sensing and Field Validation for Geological and Structural Mapping of Neoproterozoic Basement Rocks in Northern Somalia

Ahmed Nur Dalmar

ahmeddalmar3@gmail.com

Hormuud University

Research Article

Keywords: Remote Sensing, Landsat 8, Lithological Mapping, Northern Somalia, East African Orogen

Posted Date: March 20th, 2026

DOI: https://doi.org/10.21203/rs.3.rs-9127447/v1

License: This work is licensed under a Creative Commons Attribution 4.0 International License.
Read Full License

Additional Declarations: The authors declare no competing interests.

Integrated Remote Sensing and Field Validation for Geological and Structural Mapping of Neoproterozoic Basement Rocks in Northern Somalia

Ahmed Nur Dalmar[1*]

[1]Department of Geology, Faculty of Geoscience and Environment, Hormuud University, Muqdishu 204, Somalia

*Corresponding author: ahmeddalmar3@gmail.com

Abstract

The Northern Somali Basement (NSB) represents a critical segment of the East African Orogen (EAO); however, it remains poorly mapped owing to a lack of geological investigations. This study employs an integrated approach, combining Landsat 8 Operational Land Imager (OLI) multispectral data with systematic field investigations, to investigate the geological and structural framework of the Milxo area in northern Somalia. Image enhancement techniques, including principal component analysis (PCA) and specialized band ratios (Sabin's and Kaufmann's), were used to delineate lithological units and hydrothermal alteration zones. The results successfully discriminated younger granite intrusions from the surrounding Inda Ad complex metasediments, revealing that these granites occur as several isolated, smaller outcrops rather than the two large plutonic bodies depicted in legacy maps. Structural analysis identified a complex network of NE-SW and NW-SE trending lineaments and a major anticlinal fold, reflecting intense deformation during the Pan-African Orogeny. Fieldwork investigations further validated these findings, documenting phaneritic granitic textures, angular unconformities, and quartz veins. Notably, localized copper mineralization was observed along the identified fracture systems, suggesting strong structural control over mineral deposition. These results illustrate that combining satellite-based remote sensing with field validation offers an effective and economical method for geological mapping and mineral exploration in under-researched areas like Somalia.

Key Words

Remote Sensing, Landsat 8, Lithological Mapping, Northern Somalia, East African Orogen

Introduction

Remote sensing is the process of detecting and monitoring the physical and compositional characteristics of the Earth's surface by measuring the radiation it reflects or emits from a distance [20, 5]. When combined with geographic information systems (GIS), it becomes a powerful approach for geological mapping and mineral exploration [13, 18, 29]. These integrated techniques allow researchers to analyze large and inaccessible areas efficiently and provide valuable information about lithological units, structural features, and hydrothermal alteration zones. Through spectral analysis of satellite imagery, remote sensing enables the identification of lithological boundaries and alteration minerals associated with mineralization processes [27, 28, 31, 32]. In addition, remote sensing is widely used to analyze vegetation patterns, lineament extraction, drainage patterns, and other essential features [12, 15].

Over the past few decades, remote sensing has gained increasing importance in mineral exploration because of its cost-effectiveness and ability to analyze inaccessible and complex terrains [4]. Open-source multispectral satellite imagery, such as Landsat, ASTER, and Sentinel-2, provides valuable spectral information that can identify rocks and minerals, making it a powerful tool for regional-scale geological mapping and more importantly mineral exploration [14, 30, 33]. In this study, we utilized the Landsat 8 Operational Land Imager (OLI) to differentiate lithological features and create geological maps of basement complexes. Owing to its high spectral and spatial resolution, it enables the identification of rock types, hydrothermally altered zones, and structural features, making it suitable for mapping in areas with limited accessibility [12, 22]. Northern Somalia represents a record of Neoproterozoic tectonic evolution associated with the Pan-African orogeny and hosts Precambrian basement complexes that are considered prospective for mineral resources [19, 34]. These basement rocks are widely exposed along the coastal ranges known as the Golis Mountains and are mostly composed of metasedimentary sequences with minor meta-igneous units and plutonic complexes [19, 34]. Despite their geological significance, the basement terrains of Somalia remain poorly studied compared with neighboring regions, such as Ethiopia and Yemen. The collapse of Somalia’s central government in 1991 led to a sustained disruption of systematic geological surveys and mineral resource evaluations. Consequently, much of the country's geological data are based on legacy maps, which frequently lack the detail necessary for contemporary mineral exploration. In such data-deficient contexts, remote sensing serves as an effective tool for regional geological investigations and the preliminary identification of potential mineral zones.

However, remote sensing techniques have certain limitations, particularly in regions where bedrock is obscured by substantial regolith, vegetation, or other surface materials [8]. Therefore, satellite-based interpretations must be supplemented with field investigations to ensure accurate geological interpretations [9]. In this study, Landsat 8 OLI images were combined with field data to differentiate lithological units, identify structural characteristics, and locate hydrothermal alteration zones

The objectives of this study were to (1) evaluate the effectiveness of Landsat 8 OLI data for lithological discrimination in the basement complexes of northern Somalia, (2) map structural features and lineaments that may control

mineralization, and (3) validate remote sensing interpretations through field investigations to produce an updated geological map that supports future mineral exploration in the region.

Geology of the study area

The geological evolution of northern Somalia reflects its position within the East African Orogen (EAO), a Neoproterozoic to early Cambrian mobile belt associated with the assembly of Gondwana [11, 16]. The EAO is commonly subdivided into two main domains: the northern Arabian-Nubian Shield and the southern Mozambique Belt [11]. The basement of Somalia lies geographically between the juvenile terrains of the Arabian-Nubian Shield to the north and the high-grade metamorphic rocks of the Mozambique Belt to the south, forming a transitional zone within the East African Orogen (Fig. 1). These basement rocks are exposed in two main region: the Bur region in the southern Somalia and the northern coastal ranges [17]. The latter known as the Northern Somali Basement (NSB). The NSB is composed of seven major lithological units including five metasedimentary sequences and two plutonic complexes [19].

In the study area, the stratigraphy is dominated by the Inda Ad complex, which represents part of the NSB. This complex composed of low-to very low-grade metasedimentary rocks, mainly mudstone, siltstone, quartzites and carbonates [17, 21, 34] (Fig. 2). The Inda Ad Complex is notably intruded by Younger Granites interpreted as post-tectonic granitoids. Radiometric dating indicates that these granitic intrusions formed between 550 and 515 Ma, representing late Pan-African post-tectonic granites emplaced during the transition from the Neoproterozoic to the early Cambrian [10, 19].

The Mesozoic–Cenozoic succession begins with a several-meter-thick sandstone unit known as the Adigrat Sandstone, which rests unconformably on the Precambrian basement in Somalia and extends regionally into Ethiopia and Eritrea [1].

Materials and Methods

Landsat 8 Data

The study employed Landsat 8 imagery acquired by the Operational Land Imager (OLI) and Thermal Infrared Sensor (TIRS) instruments aboard the Landsat 8 platform. The dataset (LC8, Path 162 and Row 052) was acquired on April 4, 2022, and downloaded from the United States Geological Survey (USGS) EarthExplorer database. A flowchart of the adopted methodology is shown in (Fig. 3).

Digital Image Pre-Processing

Before analysis, the Landsat-8 imagery underwent standard preprocessing steps to ensure accurate interpretation. This process involved radiometric correction to reduce sensor-related noise and atmospheric correction to minimize the effects of atmospheric scattering and absorption. The Landsat-8 OLI sensor includes 11 spectral bands covering the

visible, near-infrared (NIR), shortwave infrared (SWIR), and thermal infrared regions. Bands 2-4 distinguish soil, vegetation, and rock types; Band 5 (NIR) highlights drainage patterns and moisture variations; and Bands 6-7 (SWIR1 and SWIR2) are used for geological mapping, enhancing lithological and structural mapping.

Digital Image Processing

Image processing techniques are employed to transform multispectral satellite data into images that emphasize geological features against the surrounding background. In this study, methods such as band composites, band ratios, and principal component analysis (PCA) were applied to extract spatial and spectral information relevant to lithology, structural features, and hydrothermally altered zones.

RGB Combination

Landsat imagery consists of separate grayscale bands that can be combined using the red, green, and blue (RGB) channels to create multispectral color images. The selecting of any three specific band combinations enhances the visualization of geological features, tailored to the spectral properties of minerals [25]. This study tested various RGB combinations for targeted goals, such as RGB 7-6-5, which clearly delineates lithological units.

Band Ratio

Band ratio is a technique that involves dividing the digital values of one spectral band by another to emphasize surface features often obscured in raw bands [12]. This enhances contrast and highlights mineral composition [6, 12]. In the case of Landsat 8 data, certain minerals show unique patterns; for example, clays (illite, kaolinite, and montmorillonite) low reflectance (absorption) in SWIR 2 (2110-2290 nm) but lower absorption in SWIR 1 (1570-1650 nm), whereas iron oxides and sulfates reflect highly near red (640-670 nm) and weakly in blue (450-510 nm) [12]. By applying specific band ratios, it is possible to discriminate hydrothermally altered rocks from unaltered areas. RGB composites generated these band ratios can effectively produce colored images that assist in the identification and differentiation of lithological units [23]. In this study, Sabin's ratio (4/2, 6/7, 6/5) and the Kaufmann's ratio (7/5, 5/4, 6/7) were applied (Fig. 6).

Principal Component Analysis

also known as Karhunen-Loeve analysis, is a multivariate statistical technique that transforms correlated spectral bands into a set of uncorrelated components called principal components (PCs) [2, 23]. This process enhances and distinguishes the spectral signatures from the background, facilitating the interpretation of multispectral imagery [30]. PCA reduces redundancy in highly correlated datasets and compresses information, allowing subtle variations in rocks, vegetation, and altered minerals to be detected. It can be applied to all spectral bands or selectively to bands sensitive to specific features, such as iron- or clay-bearing minerals, to effectively highlight hydrothermal alteration zones and lithological variations [12].

Results and Discussion

Color image composite

The application of Landsat-8 Operational Land Imager (OLI) False Color Composites (FCC) and Principal Component Analysis (PCA) effectively delineates the complex geological framework of the study area. Various RGB band combinations were tested to generate color composite images from the Landsat-8 OLI data. Among these, the 7-6-5 (RGB) false-color composite proved to be the most effective for lithological discrimination. This combination is particularly adept at distinguishing lithological units, geological structures, and hydrothermal alteration zones (Fig. 5 a). These wavelengths are sensitive to mineralogical variations and moisture content, thereby enhancing the identification of different rock types and surface materials. In this composite, granite outcrops are characterized by dark brown tones with massive textures, whereas metasediments appear dark gray, highlighting regional structural trends. The Meso-Cenozoic rocks exhibit mottled blue-gray hues, while conglomerate and alluvial sands are represented by light grey to off-white spectral signatures (Fig. 5a).

PCA was applied to Landsat-8 OLI bands 2-7 to reduce spectral redundancy and enhance subtle spectral variations among surface materials. PCA transforms the original multispectral data into a new set of uncorrelated components that concentrate most of the spectral information into fewer bands, thereby improving the discrimination of lithological units and geological structures [3, 26].

The RGB composite of PC7-PC6-PC5 provided the best enhancement of lithological variation within the study area (Fig. 5b). In this composite, a sharp lithological contact were observed in all lithological units more specifically contact between Inda Ad basement and Adigrat sandstone. This contact is marked by an abrupt in spectral tone and texture, appearing as green line in the left corner of (Fig. 5b. The granite outcrops are highlighted in vibrant neon green to cyan, providing a sharp contrast against the metasediments in the center of the image. Conglomerate and alluvial deposits are isolated in bright yellow to lime-green hues (Fig. 5b.

Band Ratio Analysis

The band ratio technique was applied to Landsat 8 OLI data to enhance lithological differences and highlight potential hydrothermal alteration zones [22, 35]. In band ratio images, brighter pixels represent higher ratio values and, therefore, a stronger presence of the target minerals [7] (Fig. 4). The B4/B2 ratio enhances ferric iron minerals such as hematite and limonite, which appear as bright pixels due to their high reflectance in the red band and lower reflectance in the blue band. In the study area, the Conglomerate, Alluvial deposits, and Adigrat Sandstone exhibit relativity bright due to ferruginous content, while the metasedimentary rocks of the Inda Ad Complex appear relatively darker (Fig. 4a).

The B6/B7 ratio is sensitive to hydroxyl-bearing minerals such, as clays. These minerals exhibit relatively high reflectance in Band 6 and absorption in Band 7, resulting in bright pixels in the ratio image (Fig. 4b). Consequently,

the Inda Ad Complex appears bright due to the presence of metasediments and clay-rich weathering products, whereas granite appears darker.

The B6/B5 ratio highlights ferrous iron minerals, this ratio appears brighter across the Inda Ad Complex, clearly emphasizing the bedding, deformation patterns, and elongated lithological belts of the metasedimentary rocks (Fig. 4c). RGB composites derived from these ratios were used to characterize mineral alteration, specifically granitic intrusions from the surrounding metasediments (Fig. 6). Sabin's ratio (R: 4/2, B: 6/7, G6/5) the light pink tones in the top-central part of the image mainly correspond to conglomerates and alluvial sand deposits (Fig. 6a). These sediments occur primarily in valley floors and low-lying areas where erosion products from surrounding highlands accumulate. The dark pink halos near the center of the image indicate a granitic intrusion, whereas the surrounding blue and green tones correspond to the metasedimentary of the Inda Ad Complex (Fig. 6a). (Fig. 6a).

In addition, The Kaufmann ratio composite (R:7/5, G:5/4, B:6/7) was applied to enhance lithological discrimination. In this composite, the Inda Ad Complex metasediments appear as dark green to brownish elongated belts (Fig. 6b). The contact between the granite and the Inda Ad complex is distinctly delineated in this ratio composite. The Kaufmann ratio more clearly accentuates metamorphic units and their deformation compared to Sabin's ratio (Fig. 6b).

Geology and Structure

The regional geology of the study area is dominated by Precambrian metasediments of the Inda Ad Complex, which form the main basement unit across the region. The basement rock primarily consist of low-grade metamorphic sediments, including mudstone, siltstone, quartzites, and carbonates, and phyllites are also observed in the Milxo village (Fig. 2).

The basement rocks are stratigraphically overlain by sedimentary units belonging to the Ahl Madow Group, which mainly comprises sandstones, limestones, and marlstones of Jurassic age. The sharp contact between these units can be clearly observed in (Fig. 5b), representing an unconformity. Additional early Miocene sedimentary deposits including conglomerates and sands are also overlie the older Inda Ad complex (Fig. 5).

Previous geological studies have mapped these granitic bodies as two separate intrusive plutons within the study area [1] (Fig. 2). However, the integration of multispectral Landsat-8 analysis coupled with high-resolution satellite imagery indicates that the granitic rocks occur as several isolated outcrops distributed across the central and eastern sectors of the study area (Fig. 9).

In the Sabin's ratio composite (RGB: 4/2, 6/7, 6/5), these granitic bodies appear as distinct spectral anomalies contrasting with the surrounding metasedimentary rocks and sedimentary deposits (Fig. 6a). High-resolution Google Earth imagery further supports this interpretation, showing multiple reddish patches corresponding to exposed granitic bodies that form resistant topographic highs within the landscape (Fig. 8b-c). These observations suggest that the granite distribution is more complex than that previously mapped, and consists of multiple separated exposures rather than only two large plutonic bodies.

The structural framework of the study area is strongly controlled by deformation within the Inda Ad Complex. Multispectral band analysis highlighted a prominent large-scale anticlinal fold structure located in the eastern-central region of the study area (Fig. 4c). The geometry of this structure indicates that significant compressional tectonic forces significant compressional tectonic forces that affected the basement rocks prior to or during the emplacement of the granitic intrusions.

Further structural evidence is provided by lineament extraction analysis (Fig. 7), which reveals a dense network of fractures and faults across the study area. The highest lineament density occurs within the Inda Ad Complex and along the margins of the younger granite bodies. The directions of lineaments are predominantly NE-SW and NW-SE, indicating a regional stress regime responsible for brittle deformation within the basement rocks. The intersection zones of these lineaments are particularly important because they can act as pathways for hydrothermal fluids and are therefore favorable locations for mineralization [36]. Many of these structurally controlled zones coincide with areas where artisanal gold mining activities occur, along with other minerals such as galena and copper.

Field observation

The remote sensing interpretations were verified through field observations, and results show a strong agreement between the Landsat 8 based analysis and the geological conditions observed on-site. Similar integrated approaches combining remote sensing and field validation have been widely used in mineral exploration and geological mapping [12, 14, 24, 25]. The tectonic complexity identified through multispectral band analysis and lineament extraction was confirmed by the presence of strongly tilted and folded rocks within the Inda Ad Complex (Fig. 8).

These structures are clearly visible in the field (Fig. 8b), where the rock layers show steep dips that match the regional stress pattern responsible for the mainly NE-SW and NW-SE lineament trends. The lithological interpretations were also validated, as the spectral signatures mapped as Younger Granites correspond precisely to the massive, reddish-weathering granitic outcrops with granular textures observed on-site (Fig. 8a-d). These granitic outcrops are separated across the area, consistent with the pattern observed in the satellite data (Fig. 9a-d).

Field observations further confirmed the stratigraphic relationships interpreted from the satellite imagery. A distinct angular unconformity was identified where conglomerates and alluvial sands overlie the Inda Ad Complex (Fig. 8c). Additionally, the Adigrat sandstone was observed resting unconformity above the older rocks of the Inda Ad Complex (Fig. 8f). Field evidence also documented the presence of quartz veins and traces of copper mineralization (Fig. 8e-g). These occurrences are typically localized along the identified fractures and structural zones, which served as crucial pathways for mineral-bearing hydrothermal fluids to migrate and deposit minerals within the host rocks.

Conclusion

The integration of Landsat 8 OLI remote sensing data with field-based investigations provided an improved understanding of the geological and structural framework of the study area in northern Somalia. Through multispectral analysis, including band ratios and Principal Component Analysis (PCA), to delineate lithological boundaries and identify complex structural. The remote sensing interpretations were subsequently validated through field observations. The results clearly distinguish Younger Granite intrusions from the surrounding metasedimentary rocks of the Inda Ad basement rocks. Remote sensing analysis revealed that the granitic bodies occurs as several isolated outcrops rather than as two large intrusive bodies previously mapped in earlier geological studies. Additionally, Structural analysis also identified a major anticlinal fold and dense NE-SW and NW-SE trending lineaments, indicating strong tectonic deformation and newly recognized structural features in the study area.

Field observations confirmed the remote sensing interpretations, including folded metasedimentary rocks, granitic intrusions, unconformities, quartz veins, and traces of copper mineralization. These mineral occurrences along fractures are consistent with artisanal mining activities targeting gold, galena, and copper in the area. Overall, the integration of remote sensing and field validation provides an effective and cost-efficient approach for geological mapping and mineral exploration in poorly studied regions such as Somalia.

Author Contribution

Ahmed Nur Dalmar (A.N.D.): Conceptualization, methodology, software, formal analysis, visualization, field investigation, writing-original draft preparation, and review.

Funding

This research received no external funding.

Data availability

All data generated or analyzed during this study are included in this published article.

List of Figures

Fig. 1 (a) Geographical location of Somalia. b) Study area Milxo Village northern Somalia.

Fig. 2 Geological map of the study area showing Inda Ad complex, Younger Granites, and sedimentary sequences including the Ahl Madow Group.

Fig. 3 Flowchart of the adopted methodology

Fig. 4 Band ratio grayscale images: (a) B4/B2 highlighting iron oxides; (b) B6/B7 emphasizing hydroxyl and carbonate minerals; (c) B6/B5 enhancing ferrous minerals.

Fig. 5 RGB image combinations used for lithological interpretation: (a) 7–6–5 (RGB) false-color composite; (b) Principal Component Analysis (PCA) image displayed using a 6–5–7 (RGB) band combination.

Fig. 6 RGB composite band ratios for hydrothermal alteration mapping: (a) Sabin's ratio using 4/2, 6/7, 6/5 (RGB); (b) Kaufmann ratio using 7/5, 5/4, 6/7 (RGB).

Fig. 7 Surface Lineament Map of the Study Area

Fig. 8 Geological Field Observations photos (a) Young Granite Intrusion: reddish-weathered granitic body forming a distinct topographic high. (b) Deformation in Inda Ad Series (c) Angular Unconformity: showing a sharp contact (yellow line) where modern conglomerate and alluvial sand deposits overlie the tilted Inda Ad basement. (d) Close-up of Young Granite: showing the phaneritic texture of the younger granitic intrusion. (e) Localized secondary copper mineralization (likely malachite or azurite) appearing as greenish traces within the host rock along with small quartz veins. (f) A distinct boundary (yellow line) between the basal Adigrat Sandstone and the underlying older Inda Ad formation. (g) Iron-stained quartz boulder indicating the presence of hydrothermal quartz veining in the area.

Fig. 9 Identification of granite a) landsat 8 Sabin's ratio composite showing revised granite outcrops (yellow). (b-c) high resolution Google Earth images showing granite outcrops as reddish weathered surfaces. (a) field photograph of weathering granite outcrops.

296

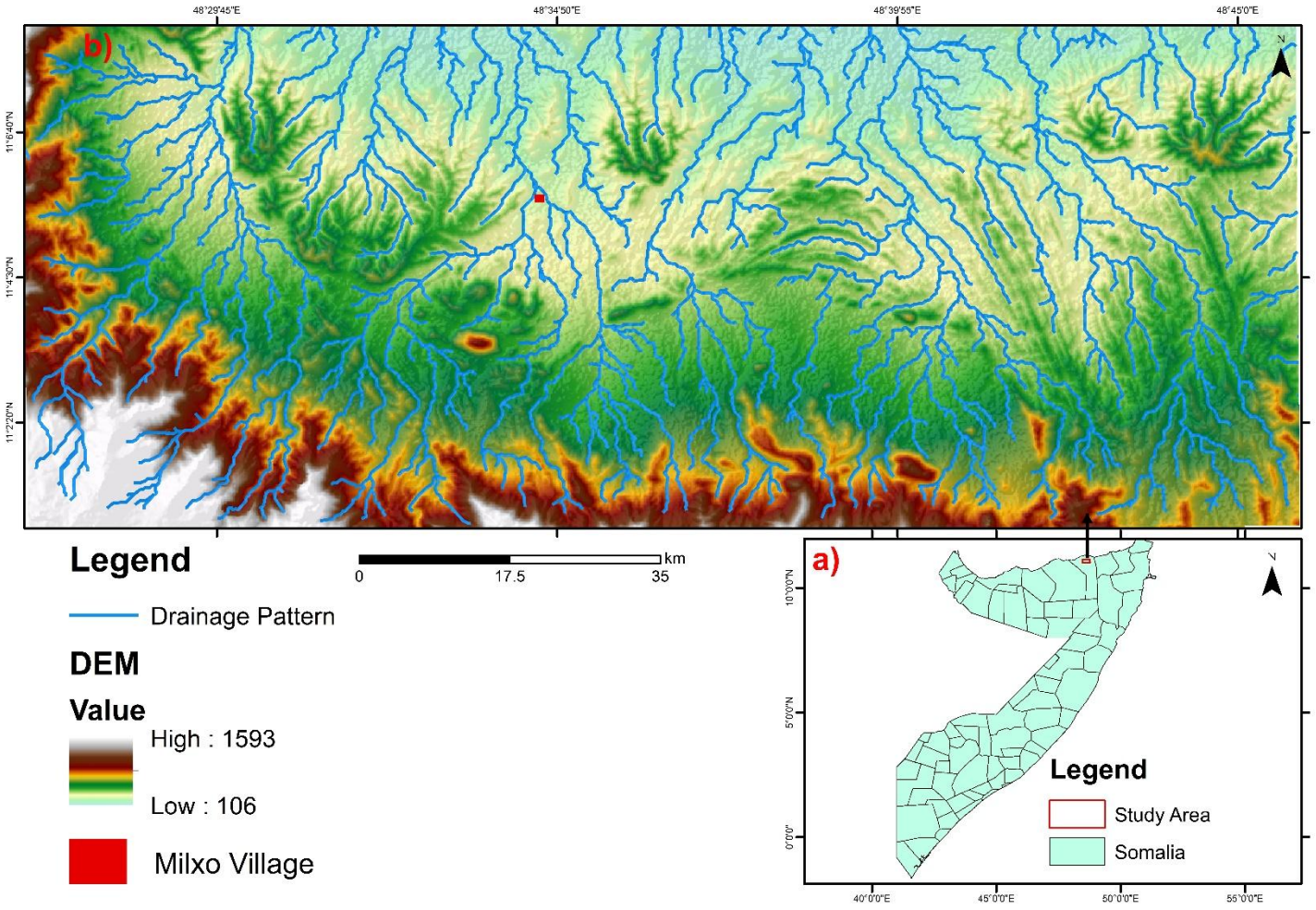

297

298 **Fig. 1**

299

300

301

302

303

304

305

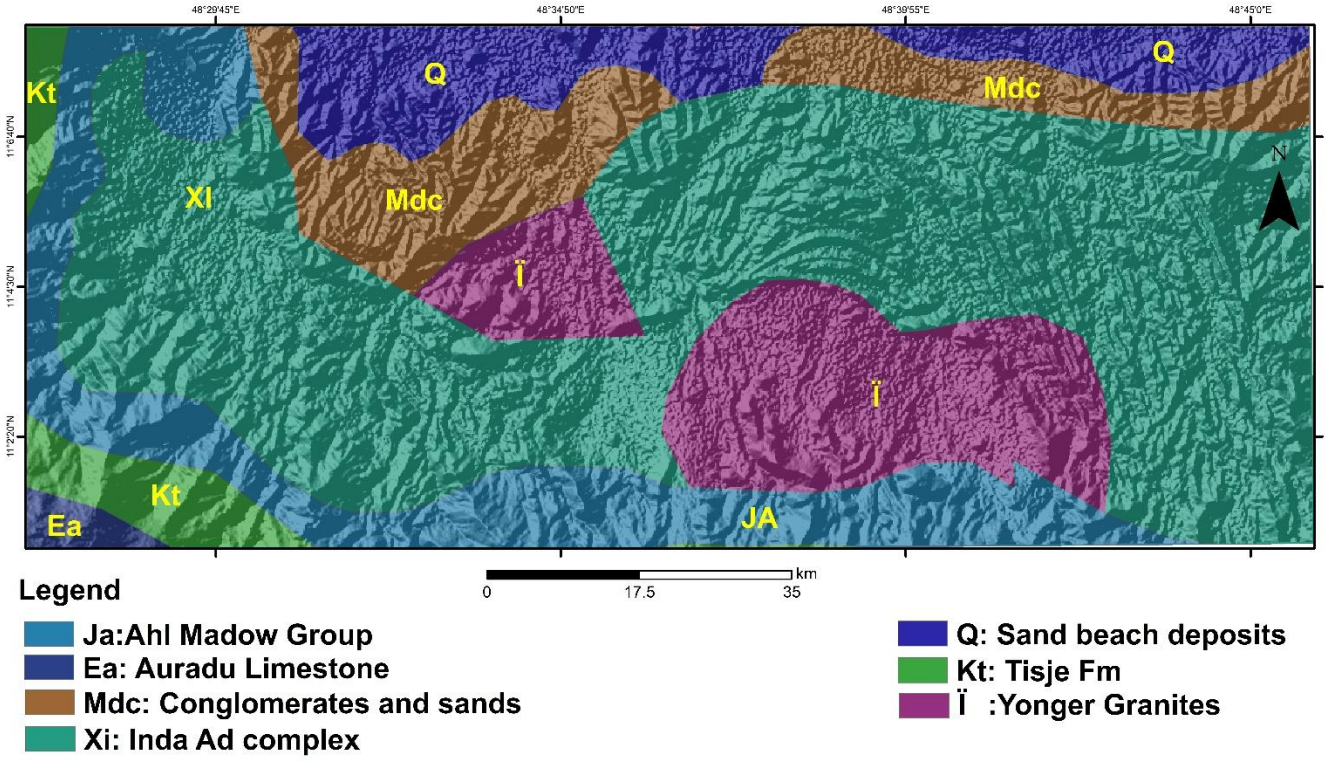

306

307 **Fig. 2**

308

309

310

311

312

313

314

315

316

317

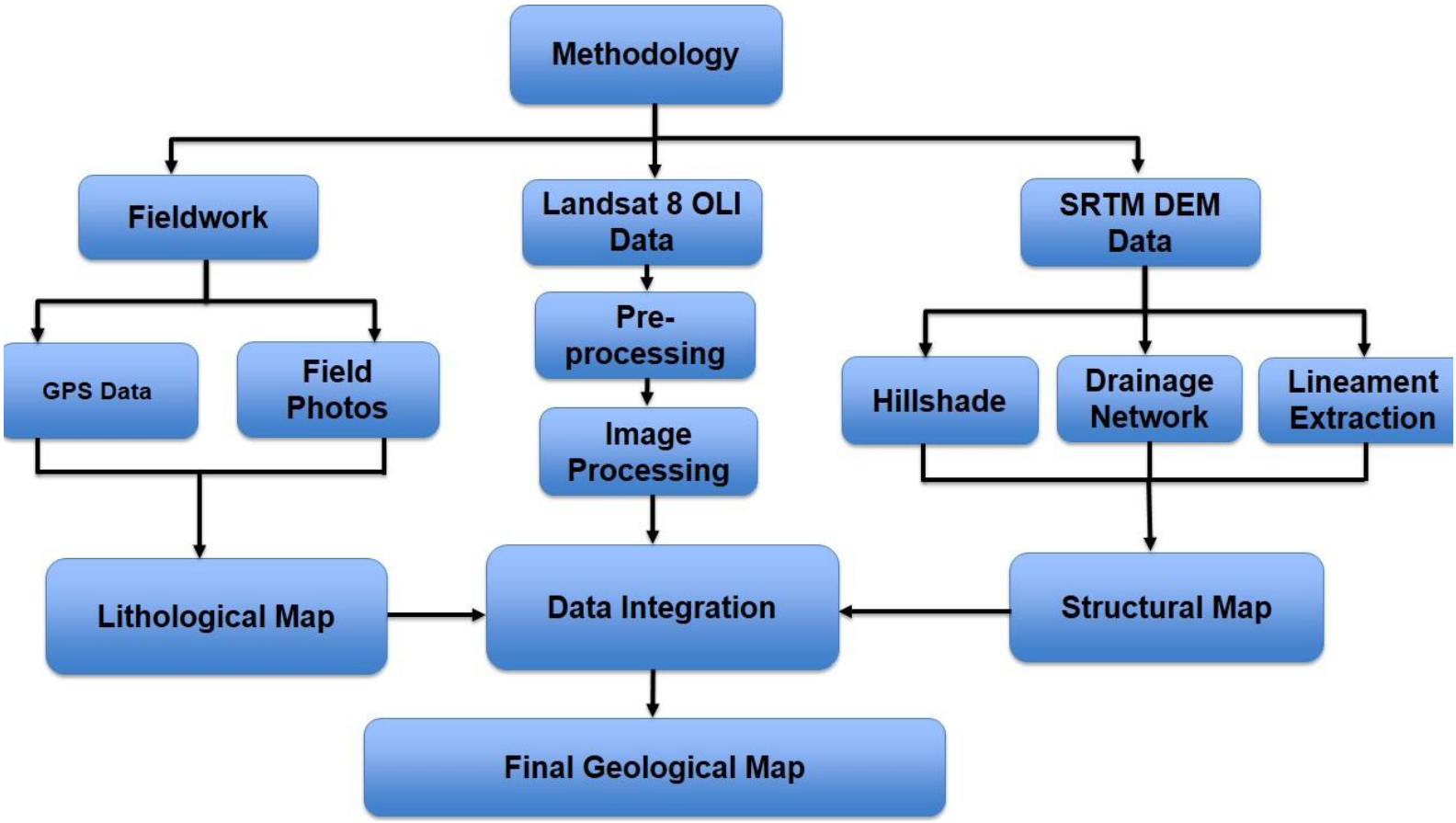

318

319 **Fig. 3**

320

321

322

323

324

325

326

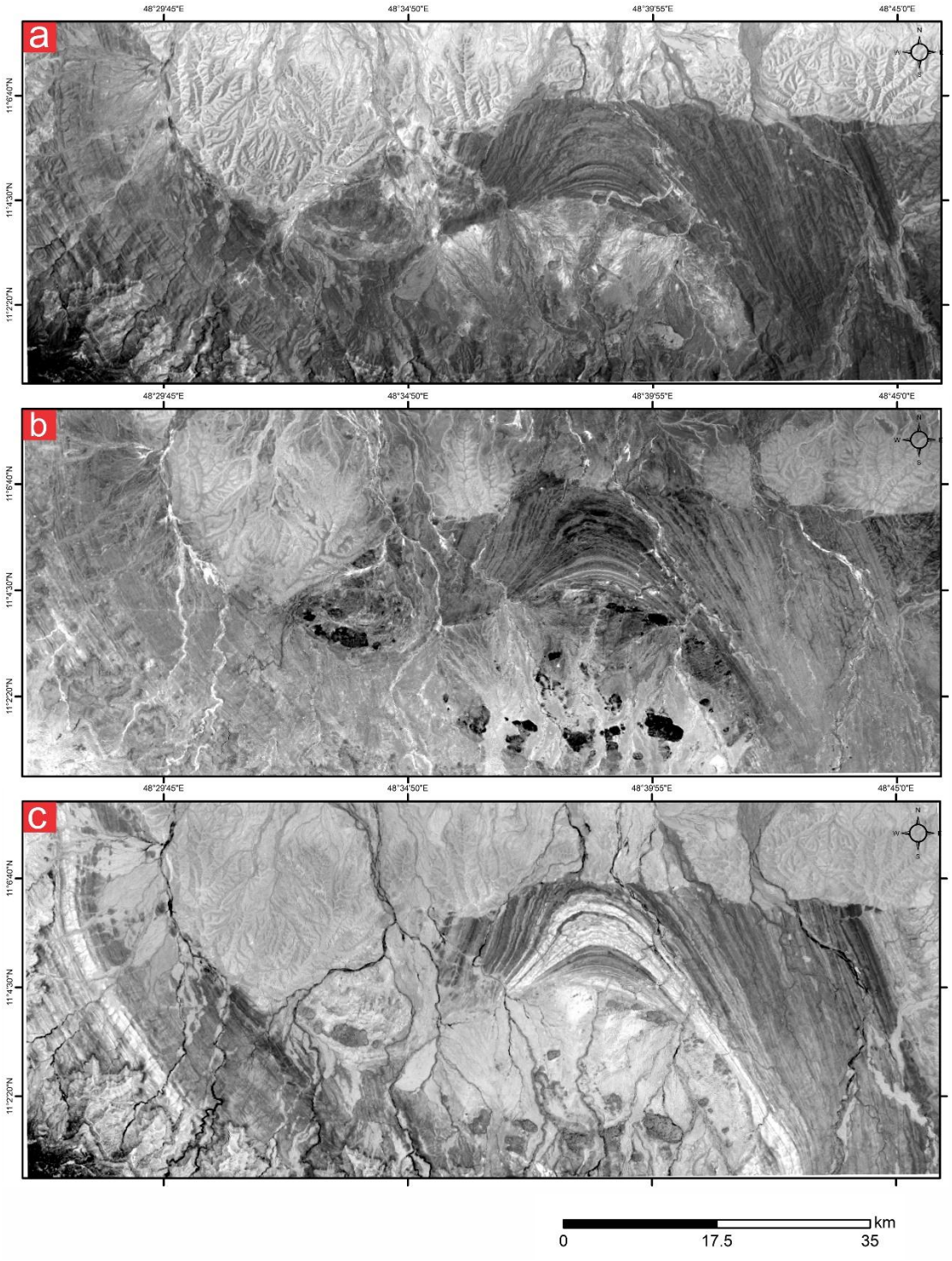
a
b
c
48°29'45"E
48°34'50"E
48°39'55"E
48°45'0"E
11°6'40"N
11°4'30"N
11°2'20"N
N
W
E
S
km
0
17.5
35

Fig. 4

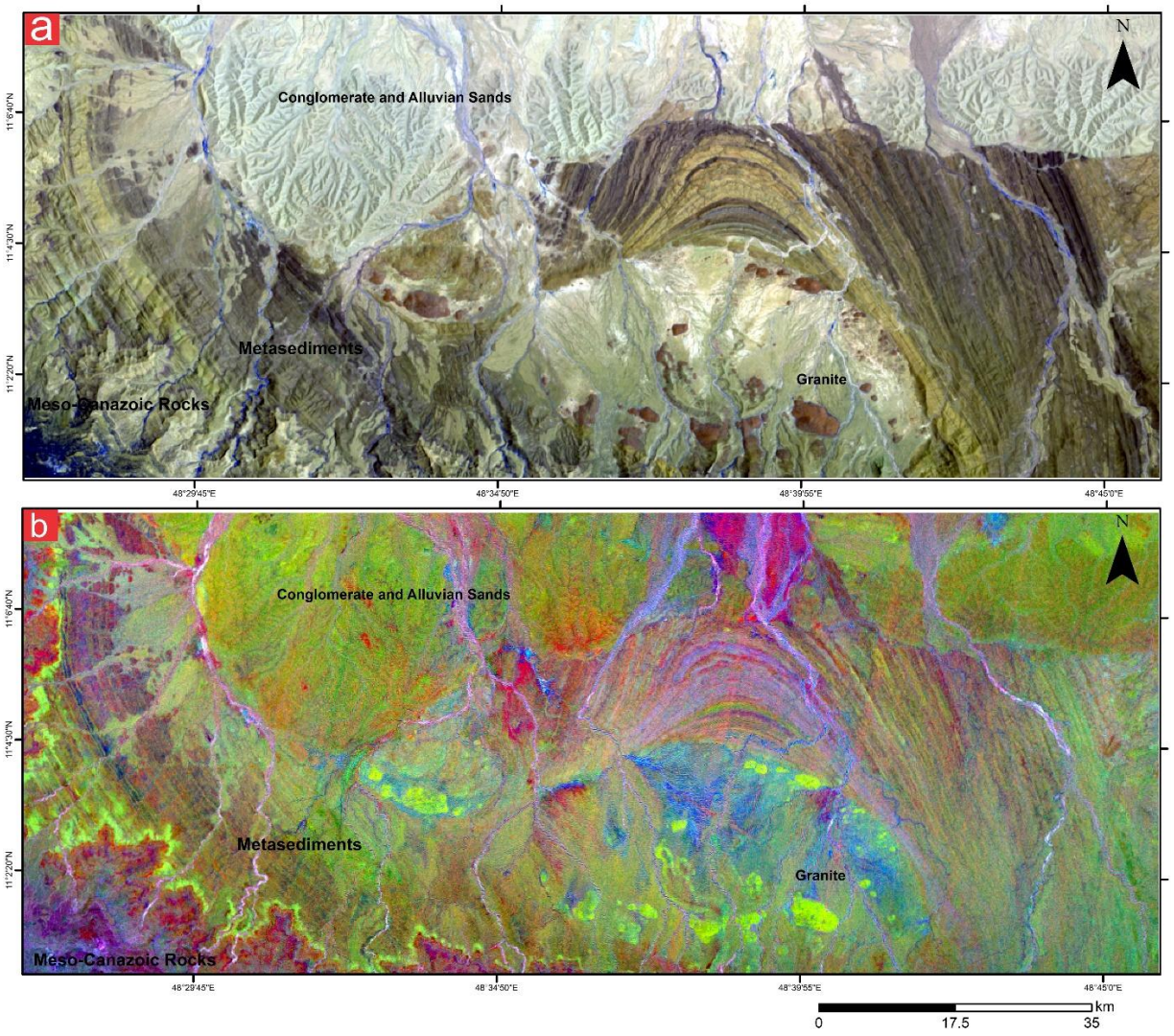
a
N
Conglomerate and Alluvian Sands
Metasediments
Granite
Meso-Canazoic Rocks
11°6'40"N
11°4'30"N
11°2'20"N
48°29'45"E
48°34'50"E
48°39'55"E
48°45'0"E
b
N
Conglomerate and Alluvian Sands
Metasediments
Granite
Meso-Canazoic Rocks
11°6'40"N
11°4'30"N
11°2'20"N
48°29'45"E
48°34'50"E
48°39'55"E
48°45'0"E
km
0
17.5
35

Fig. 5

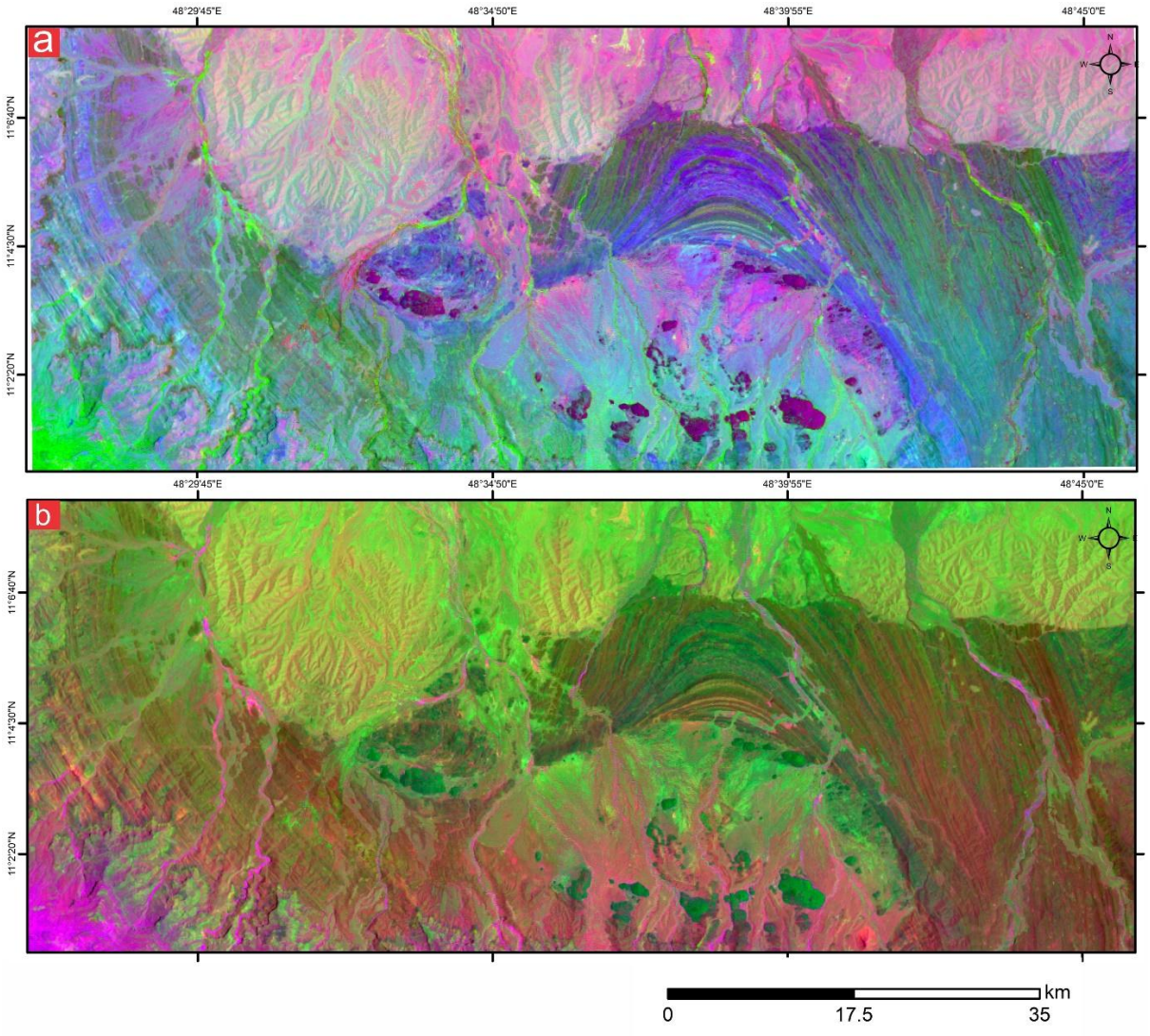
a
b
48°29'45"E
48°34'50"E
48°39'55"E
48°45'0"E
11°6'40"N
11°4'30"N
11°2'20"N
N
W
E
S
km
0
17.5
35

Fig. 6

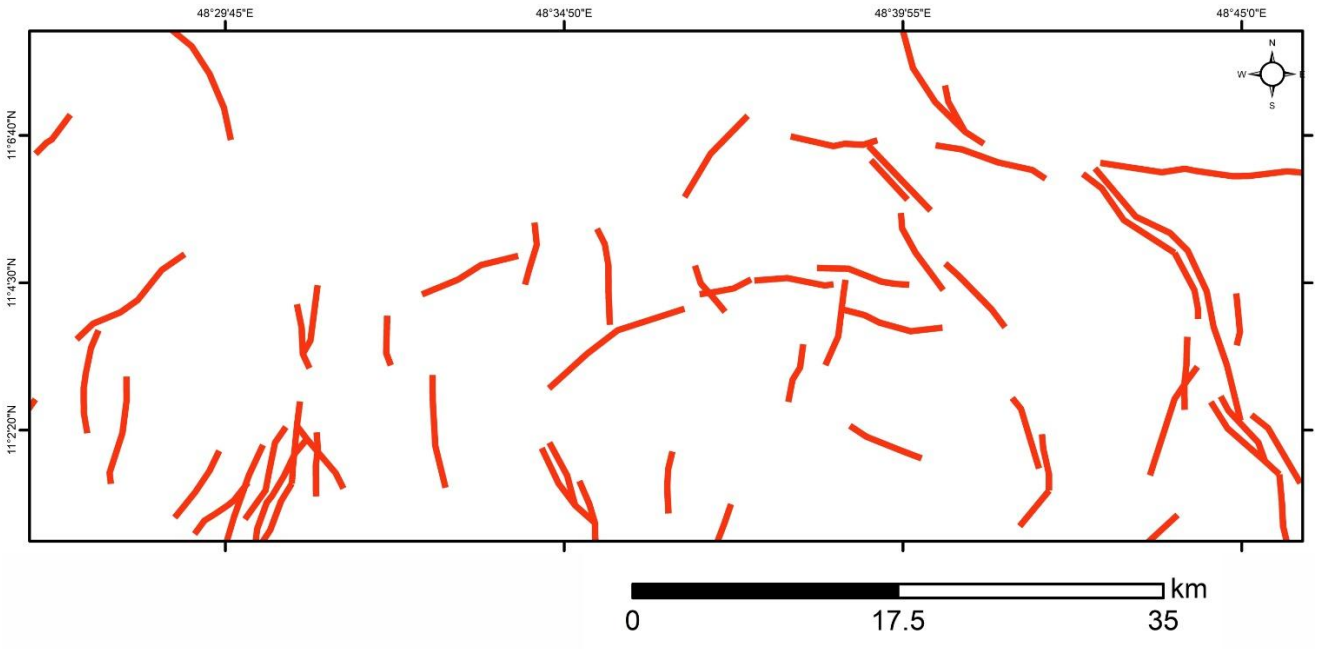
48°29'45"E
48°34'50"E
48°39'55"E
48°45'0"E
11°6'40"N
11°4'30"N
11°2'20"N
N
W
E
S
km
0
17.5
35

Fig. 7

365

366 **Fig. 8**

367

368

369

370

371

372

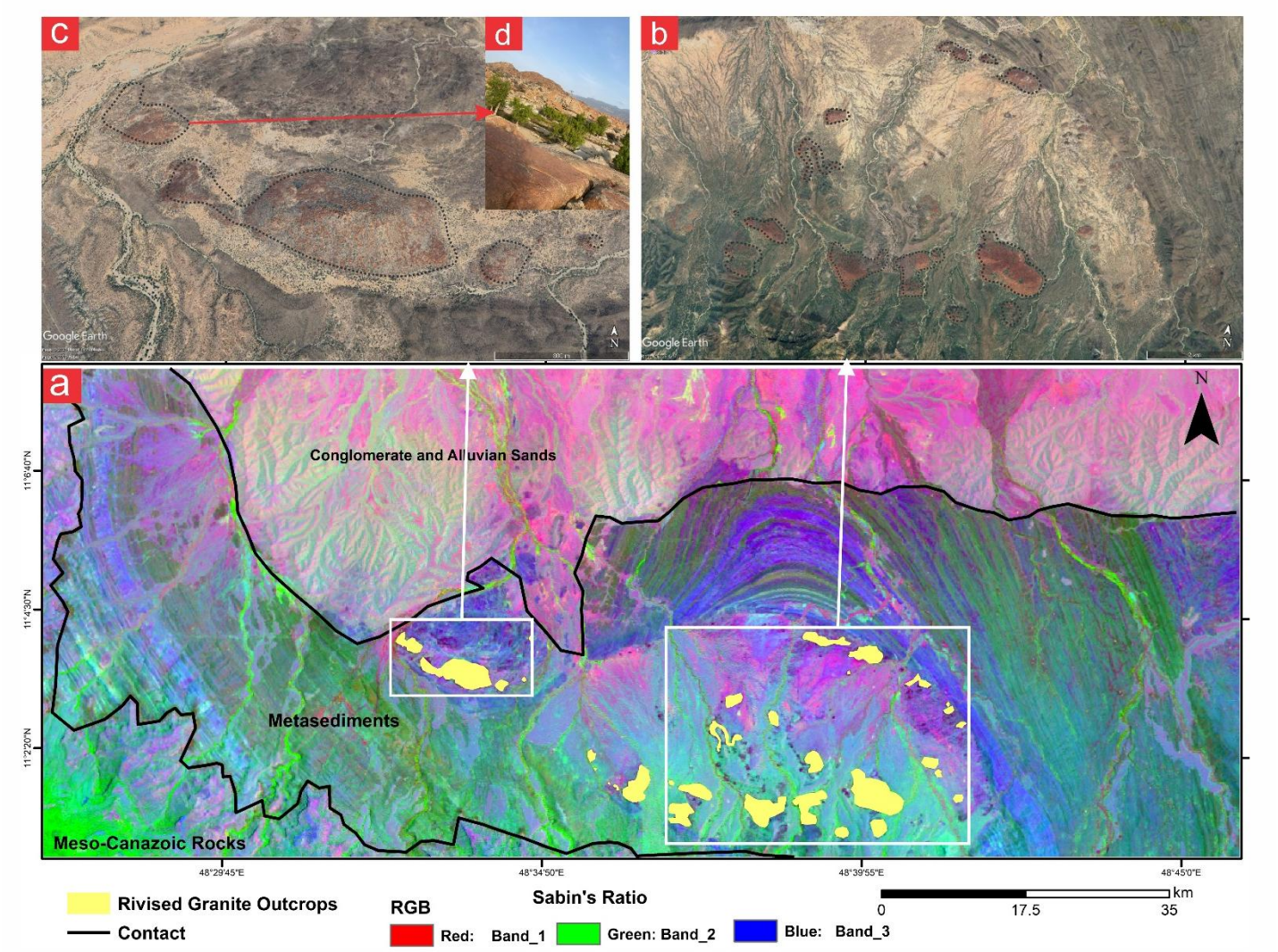

373

374 **Fig. 9**

375

376

377

References

[1] Abbate E, Bruni P, Sagri M (2015) Geology of Ethiopia: a review and geomorphological perspectives. Landscapes and landforms of Ethiopia: 33–64. https://doi.org/10.1007/978-94-017-8026-1_2

[2] Abd El-Wahed M et al. (2023) Multisensor satellite data and field studies for unravelling the structural evolution and gold metallogeny of the Gerf Ophiolitic Nappe, Eastern Desert, Egypt. Remote Sensing 15(8):1974. https://doi.org/10.3390/rs15081974

[3] AbdelMaksoud KM, El-Arafy RA (2024) Using selective principal component analysis (SPCA) for lithologic mapping of different granitic phases in South Sinai, Egypt. Journal of the Indian Society of Remote Sensing 52(7):1633–1647. https://doi.org/10.1007/s12524-024-01892-4

[4] Abdulraheem MI, Zhang W, Li S, Moshayedi AJ, Farooque AA, Hu J (2023) Advancement of remote sensing for soil measurements and applications: A comprehensive review. Sustainability 15(21):15444. https://doi.org/10.3390/su152115444

[5] Adiri Z, Lhissou R, El Harti A, Jellouli A, Chakouri M (2020) Recent advances in the use of public domain satellite imagery for mineral exploration: A review of Landsat-8 and Sentinel-2 applications. Ore Geology Reviews 117:103332. https://doi.org/10.1016/j.oregeorev.2020.103332

[6] Ali AS, Pour AB (2014) Lithological mapping and hydrothermal alteration using Landsat 8 data: a case study in ariab mining district, red sea hills, Sudan. International Journal of Basic and Applied Sciences 3(3):199. https://doi.org/10.14419/ijbas.v3i3.2842

[7] Cavur M, Yu YT, Demir E, Duzgun S (2024) Mapping geothermal indicator minerals using fusion of target detection algorithms. Remote Sensing 16(7):1223. https://doi.org/10.3390/rs16071223

[8] Chen Y, Wang Y, Zhang F, Dong Y, Song Z, Liu G (2023) Remote sensing for lithology mapping in vegetation-covered regions: Methods, challenges, and opportunities. Minerals 13(9):1153. https://doi.org/10.3390/min13091153

[9] Cracknell M, Reading AM, De Caritat P (2015) Multiple influences on regolith characteristics from continental-scale geophysical and mineralogical remote sensing data using Self-Organizing Maps. Remote Sensing of Environment 165:86–99. https://doi.org/10.1016/j.rse.2015.04.029

[10] Fantozzi PL (2002) Geological mapping in northeastern Somalia (Midjiurtinia region): field evidence of the structural and paleogeographic evolution of the northern margin of the Somalian plate. Journal of African Earth Sciences 34(1-2):21–55. https://doi.org/10.1016/S0899-5362(01)00100-2

[11] Fritz H et al. (2013) Orogen styles in the East African Orogen: A review of the Neoproterozoic to Cambrian tectonic evolution. Journal of African Earth Sciences 86:65–106. https://doi.org/10.1016/j.jafrearsci.2013.06.004

[12] Frutuoso R, Lima A, Teodoro AC (2021) Application of remote sensing data in gold exploration: targeting hydrothermal alteration using Landsat 8 imagery in northern Portugal. Arabian Journal of Geosciences 14(6):459. https://doi.org/10.1007/s12517-021-06786-0

412 [13] Harris J, Wilkinson L, Grunsky E (2000) Effective use and interpretation of lithogeochemical data in regional
413 mineral exploration programs: application of Geographic Information Systems (GIS) technology. Ore Geology
414 Reviews 16(3-4):107–143. https://doi.org/10.1016/S0169-1368(99)00027-X

415 [14] Hu B, Xu Y, Wan B, Wu X, Yi G (2018) Hydrothermally altered mineral mapping using synthetic application
416 of Sentinel-2A MSI, ASTER and Hyperion data in the Duolong area, Tibetan Plateau, China. Ore Geology Reviews
417 101:384–397. https://doi.org/10.1016/j.oregeorev.2018.07.017

418 [15] Jeyaseelan AT (2003) Droughts & floods assessment and monitoring using remote sensing and GIS. Satellite
419 remote sensing and GIS applications in agricultural meteorology: 291–313.

420 [16] Johnson PR, Woldehaimanot B (2003) Development of the Arabian–Nubian Shield: perspectives on accretion
421 and deformation in the northern East African Orogen and the assembly of Gondwana. In: Yoshida M, Windley BF,
422 Dasgupta S (Eds) Proterozoic East Gondwana: Supercontinent Assembly and Breakup, Geological Society of London
423 206:289–325. https://doi.org/10.1144/GSL.SP.2003.206.01.15

424 [17] Kamenov BK, Billi P, Migoń P (2022) Inselberg Landscape of the Bur Area in Southern Somalia. In: Landscapes
425 and Landforms of the Horn of Africa: Eritrea, Djibouti, Somalia. Springer: 249–263. https://doi.org/10.1007/978-3-
426 031-05487-7_11

427 [18] Knox-Robinson C, Wyborn L (1997) Towards a holistic exploration strategy: using geographic information
428 systems as a tool to enhance exploration. Australian Journal of Earth Sciences 44(4):453–463.
429 https://doi.org/10.1080/08120099708728326

430 [19] Kröner A, Sassi F (1996) Evolution of the northern Somali basement: new constraints from zircon ages. Journal
431 of African Earth Sciences 22(1):1–15. https://doi.org/10.1016/0899-5362(95)00121-2

432 [20] Lambin EF (2001) Remote sensing and geographic information systems analysis. Methods and applications of
433 geographic information systems: 3–21.

434 [21] Mandal A, Saha D, Kumar A (2022) Structural analysis and seismic stratigraphy for delineation of
435 Neoproterozoic-Cambrian petroleum system in central and eastern part of Bikaner–Nagaur basin, India. Journal of
436 Petroleum Exploration and Production Technology 12(6):1709–1725. https://doi.org/10.1007/s13202-021-01432-7

437 [22] Masoumi F, Eslamkish T, Honarmand M, Abkar AA (2017) A comparative study of landsat-7 and landsat-8 data
438 using image processing methods for hydrothermal alteration mapping. Resource Geology 67(1):72–88.
439 https://doi.org/10.1111/rge.12117

440

441 [23] Mohamed MTA, Al-Naimi LS, Mgbeojedo TI, Agoha CC (2021) Geological mapping and mineral prospectivity
442 using remote sensing and GIS in parts of Hamissana, Northeast Sudan. Journal of Petroleum Exploration and
443 Production 11(3):1123–1138. https://doi.org/10.1007/s13202-021-01115-3

444 [24] Nafigin IO, Ishmukhametova VT, Ustinov SA, Minaev VA, Petrov VA (2022) Geological and mineralogical
445 mapping based on statistical methods of remote sensing data processing of landsat-8: a case study in the southeastern
446 Transbaikalia, Russia. Sustainability 14(15):9242. https://doi.org/10.3390/su14159242

447 [25] Pour AB, Hashim M (2015) Hydrothermal alteration mapping from Landsat-8 data, Sar Cheshmeh copper mining
448 district, south-eastern Islamic Republic of Iran. Journal of Taibah University for Science 9(2):155–166.
449 https://doi.org/10.1016/j.jtusci.2014.11.008

450 [26] Rajan Girija R, Mayappan S (2019) Mapping of mineral resources and lithological units: A review of remote
451 sensing techniques. International Journal of Image and Data Fusion 10(2):79–106.
452 https://doi.org/10.1080/19479832.2019.1589585

453 [27] Rajesh H (2004) Application of remote sensing and GIS in mineral resource mapping-An overview. Journal of
454 Mineralogical and Petrological Sciences 99(3):83–103. https://doi.org/10.2465/jmps.99.83

455 [28] Sabins FF (1999) Remote sensing for mineral exploration. Ore Geology Reviews 14(3-4):157–183.
456 https://doi.org/10.1016/S0169-1368(99)00007-4

457 [29] Saha SK (2022) Remote sensing and geographic information system applications in hydrocarbon exploration: a
458 review. Journal of the Indian Society of Remote Sensing 50(8):1457–1475. https://doi.org/10.1007/s12524-022-
459 01540-9

460 [30] Sekandari M et al. (2020) Application of Landsat-8, Sentinel-2, ASTER and WorldView-3 spectral imagery for
461 exploration of carbonate-hosted Pb-Zn deposits in the Central Iranian Terrane (CIT). Remote Sensing 12(8):1239.
462 https://doi.org/10.3390/rs12081239

463 [31] Shirmard H, Farahbakhsh R, Müller RD, Chandra R (2022) A review of machine learning in processing remote
464 sensing data for mineral exploration. Remote Sensing of Environment 268:112750.
465 https://doi.org/10.1016/j.rse.2021.112750

466 [32] Tagwai MG, Jimoh OA, Shehu SA, Zabidi H (2024) Application of GIS and remote sensing in mineral
467 exploration: current and future perspectives. World Journal of Engineering 21(3):487–502.
468 https://doi.org/10.1108/WJE-09-2022-0395

469 [33] Tompolidi AM, Sykioti O, Koutroumbas K, Parcharidis I (2020) Spectral unmixing for mapping a hydrothermal
470 field in a volcanic environment applied on ASTER, Landsat-8/OLI, and Sentinel-2 MSI Satellite Multispectral Data:
471 The Nisyros (Greece) case study. Remote Sensing 12(24):4180. https://doi.org/10.3390/rs12244180

472 [34] Whitehouse MJ, Windley BF, Stoeser DB, Al-Khirbash S, Ba-Bttat MA, Haider A (2001) Precambrian basement
473 character of Yemen and correlations with Saudi Arabia and Somalia. Precambrian Research 105(2-4):357–369.
474 https://doi.org/10.1016/S0301-9268(00)00120-0

475 [35] Yang C, Jia H, Dong L, Zhao H, Zhao M (2024) Selection of Landsat-8 operational land imager (OLI) optimal
476 band combinations for mapping alteration zones. Remote Sensing 16(2):392. https://doi.org/10.3390/rs16020392

[36] Yousefi M, Hronsky JM (2023) Translation of the function of hydrothermal mineralization-related focused fluid flux into a mappable exploration criterion for mineral exploration targeting. Appl Geochem 149:105561. https://doi.org/10.1016/j.apgeochem.2023.105561